ACS OMEGA

Open Access

http://pubs.acs.org/journal/acsodf

Article

Surface-Assisted Laser Desorption/Ionization Mass Spectrometry with a Two-Dimensional Au Nanoparticle Array for Soft Ionization

Kohei Shibamoto* and Takashi Fujita

Cite This: *ACS Omega* 2024, 9, 21822−21828

Read Online

ACCESS | Metrics & More | Article Recommendations

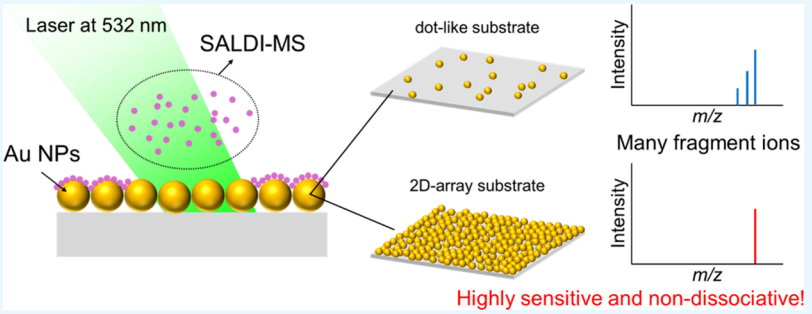

ABSTRACT: Surface-assisted laser desorption/ionization mass spectrometry (SALDI-MS) is a valuable technique for detecting small molecules in environmental and medicinal studies. We investigated dot-like and 2D-array gold nanoparticle-based SALDI-MS substrates that excite surface plasmons and enhance the desorption/ionization of sample molecules via charge transfer between the substrate and sample molecules. We aimed to optimize the nondissociative detection of sample molecules by efficiently transferring energy while suppressing excess internal energy. SALDI-MS measurements using crystal violet (CV) molecules revealed ion intensity and spectral pattern differences between the dot-like and 2D-array substrates. SALDI-MS measurements using dot-like substrates suggested two desorption/ionization processes: internal energy supply and charge transfer between the substrate and sample molecules. However, SALDI-MS measurements using 2D-array substrates suggested that the internal energy supply was suppressed. As a result, the dot-like substrate provided higher desorption/ionization efficiency but increased fragmentation, whereas the 2D-array substrate was suitable for highly sensitive and nondissociative SALDI-MS measurements. This study contributes to the optimization of SALDI-MS measurements and advances our understanding of energy transfer and sample molecule dissociation.

INTRODUCTION

Surface-assisted laser desorption/ionization mass spectrometry (SALDI-MS) has become a powerful analytical tool for detecting small molecules and has shown considerable potential in environmental and medicinal investigations.[1−3] Unlike matrix-assisted laser desorption/ionization MS (MALDI-MS), SALDI-MS does not require the addition of matrix molecules, thus eliminating background peaks from the random dissociation of matrix molecules and sweet spots because of the heterogeneity of the sample-matrix cocrystal.

SALDI-MS utilizes the absorption of laser irradiation by inorganic materials on the substrate surface to facilitate the desorption and ionization of sample molecules. This is achieved through the transfer of energy from the substrate to the analyte. The well-known mechanism of SALDI-MS involves the desorption and ionization of the sample by rapidly heating the substrate with laser irradiation, thus transferring internal energy to the sample.[4] Consequently, most SALDI-MS substrates are designed with nanoscale surface roughness to promote efficient energy transfer. However, using high laser power to enhance sensitivity often leads to increased dissociation of sample molecules due to excess internal energy. This makes the nondissociative detection and identification of sample molecules challenging. Therefore, engineering the optical, structural, and thermal properties of a nanostructure is crucial for developing a high-performance SALDI substrate.

Various substrates have been reported for SALDI-MS, including porous silicon,[5−7] other surface-roughened materials,[8] surface-modified silicon with organic molecules for capturing target molecules,[9] and nanoparticle surfaces.[10,11] Au nanoparticles (NPs) are especially promising candidates for developing SALDI-MS substrates, owing to their high chemical stability and the ease with which they can be functionalized

Received: November 7, 2023
Revised: March 7, 2024
Accepted: March 25, 2024
Published: May 9, 2024

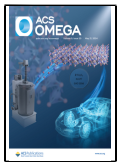

https://doi.org/10.1021/acsomega.3c08648
ACS Omega 2024, 9, 21822−21828

based on Au-thiol interactions. Several studies have successfully utilized Au NPs in SALDI-MS for biomolecular analysis, achieving the detection of low-mass metabolites with low background noise.[12−15] Moreover, the unique optical properties of Au NPs, such as surface plasmon (SP) excitation, which is the collective oscillation of electrons, contribute to the enhancement of the desorption and ionization processes in SALDI-MS.[16−18] This enhancement enables the detection of analytes at lower concentrations, making Au NPs an attractive option for trace analysis in complex biological samples.

We have previously reported on SALDI-MS substrates with Au NP dots,[16] Au thin films,[17] and TiO_2 NPs[19] that utilize energy transfer via charge transfer between the substrate and sample in addition to internal energy transfer. In the Au-based SALDI substrate, we showed that charge transfer based on SP contributes to the efficient desorption and ionization of sample molecules. We succeeded in detection of a significantly small amount of analyte molecules, less than several hundred zeptomoles using the Au NP dot substrate.[16] However, when peptides and sugars were measured with this substrate, dissociated ions were observed due to the supply of excess internal energy. On the other hand, in SALDI-MS measurements using a smooth gold film,[17] in which localized rapid heating was less likely to occur, few dissociated ions from the sample were observed, although the detection sensitivity was lower than that of the Au NP dot substrate. This result suggests that supplying energy to the sample by charge transfer may result in less dissociation than when the internal energy is transferred.

In this study, we investigated whether the efficient transfer of energy from the substrate to the sample by charge transfer, while suppressing the excess internal energy by rapid heating, would lead to the nondissociative detection of sample molecules by SALDI-MS. The first approach to testing this hypothesis is to compare the nondissociative properties of samples from two sample preparation methods that provide different adsorption types, chemisorption and physisorption, because effective charge interaction requires the chemisorption of sample molecules on the surface.[20,21] The second approach compares the thermal diffusion effect using two SALDI-MS ionization substrates. These SALDI-MS ionization substrates have different arrangements: dotted Au NPs and 2D arrays of Au NPs. A comparison of these SALDI-MS results will provide important information about the relationship between the energy transfer and dissociation of sample molecules, which will improve the SALDI-MS measurements.

EXPERIMENTAL SECTION

Au NPs in Aqueous Solution. Au NPs in an aqueous solution were purchased from British Biocell International for SP excitation. Their diameter was 60 nm with a standard deviation of 8%, and their density was 2.6×10^{10} particles/mL in an aqueous solution. Au is chemically stable, and its surface is difficult to oxidize; therefore, charge interactions would not be disturbed by surface oxidation.

Fabrication of the SALDI-MS Substrates. Two fabrication techniques were used to prepare SALDI-MS ionization substrates. First, ionized substrates were prepared by dropping the Au NP dispersion in an aqueous solution onto an n-type (100) Si wafer purchased from Nilaco. Second, as reported previously, two-dimensional Au NP arrays (2D arrays) were formed at the liquid−liquid interface and then moved onto n-type (100) Si wafers.[22,23]

Characterization of SALDI-MS Substrates. The fabricated SALDI-MS ionization substrates were characterized by using a scanning electron microscope (KEYENCE VK-9700). Their optical properties were estimated from their absorption efficiencies via an absorbance determination (SHIMADZU UV-1600).

Laser Desorption/Ionization Mass Spectrometry. The LDI-MS measurements in this study were performed in positive ionization mode using our original LDI equipment, a linear time-of-flight mass spectrometer with delayed extraction. We used a Nd:YAG pulse laser as the light source for our LDI measurements. The pulse train wavelength was 1064 nm with a repetition rate of 10 Hz and a pulse width of 8 ns. The pulses were frequency-doubled to a wavelength of 532 nm for SP excitation of the Au NPs. The laser fluence was controlled with a variable reflective neutral density filter and was set to range from 80 to 280 $\mu J/mm^2$ after laser focusing. The area of the focused laser spot was 0.5 mmφ (approximately 0.2 mm^2). Laser fluences were in the range of 80 to 280 $\mu J/mm^2$ for these SALDI-MS measurements. With a fluence of 80 $\mu J/mm^2$, the ionization substrates were irradiated with 2.0×10^{14} photons/mm^2.

Sample Molecules. Crystal violet (CV) molecules, which are known to chemisorb on Au surfaces,[24] were used as the sample molecules. The CV molecules were dissolved in water at a concentration of 50 μM.

Preparation of Sample Molecules on Ionization Substrates. Two preparation techniques for the sample molecules on the ionization substrates were used. The number of CV molecules used in the measurements was set to be equal to the number covering the Au NP surface as a monolayer (several picomoles per square millimeter). The number of adsorbed molecules was determined by estimating the surface area of Au NPs and the adsorption area of a CV molecule. A CV molecule consists of a central carbon atom connected to three phenyl rings and one CV molecule can be considered to be a circle with a diameter of 1 nm.[25] Therefore, the number density of CV molecules per unit area was estimated to be 1.3×10^{12} molecules/mm^2. During the first sample preparation technique, 1 μL of the prepared CV aqueous solution at a concentration of 50 μM was dropped onto fabricated ionization substrates. This sample preparation technique is referred to as the drop method. During the second sample preparation technique, fabricated ionization substrates were dipped into the prepared CV aqueous solution with a concentration of 50 μM. After immersion for 15 min, the ionized substrate was rinsed with deionized water to remove unabsorbed CV molecules. The 15 min immersion time was determined through surface-enhanced Raman scattering spectroscopy in our previous study of the Au NPs-CV system.[26] This sample preparation technique is termed the dip method. This procedure provided flat adsorption of the CV molecules as a single layer, while the drop technique resulted in random adsorption. In addition, this dipping method did not change the density of the Au NPs on the ionization substrate.

RESULTS AND DISCUSSION

Figure 1a shows a scanning electron microscopy (SEM) image (×18,000) of an ionization substrate prepared by the first fabrication technique. The Au NPs were dispersed randomly on a Si wafer with a density of several tens of particles per square micrometer. Although multiple substrates were fabricated, the number density of the Au NPs was consistently

https://doi.org/10.1021/acsomega.3c08648
ACS Omega 2024, 9, 21822−21828

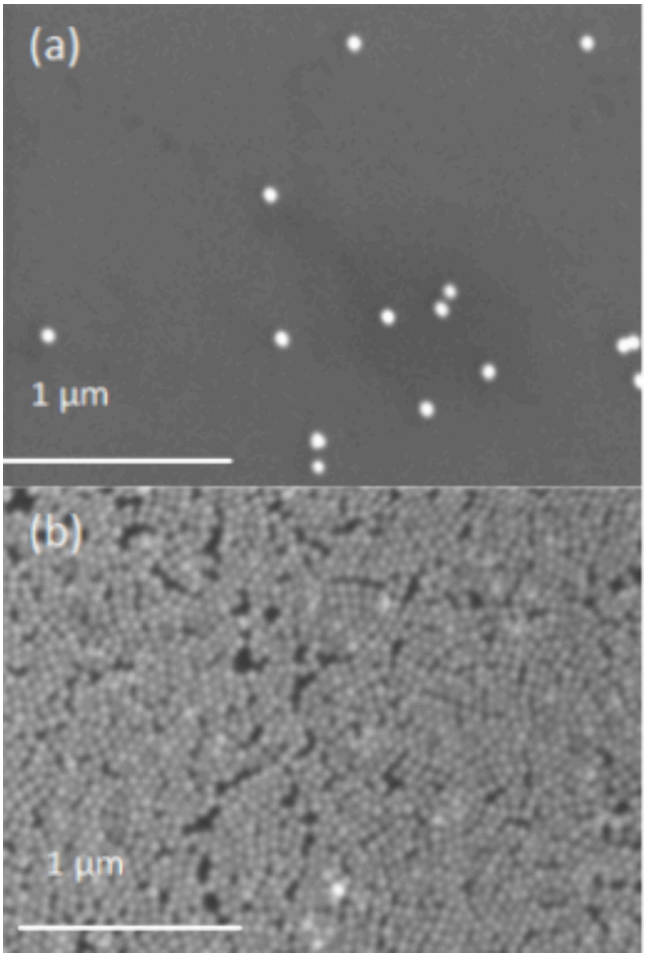

Figure 1. SEM images of Au nanoparticles with a diameter of 60 nm on Si substrates prepared using two different fabrication techniques: (a) a dot-like substrate and (b) a 2D-array substrate.

reproduced, indicating no significant differences among the prepared ionization substrates. The substrate prepared using the first fabrication technique is referred to as a dot-like substrate. Figure 1b shows an SEM image (×18,000) of the ionization substrate prepared using the second fabrication technique. The Au NPs were arranged in a plane like a 2D array, and their density was 300 particles/μm^2, which is at least ten times greater than that of the dot-like substrate. In this paper, the substrate prepared using the second fabrication technique is termed a 2D-array substrate.

The reflectance spectra of the dot-like and 2D-array substrates are shown in Figure 2 and represented by dashed and solid lines, respectively. The dot-like substrate exhibited apparent optical absorption at a wavelength of approximately 520 nm, corresponding to the SP excitation of isolated Au NPs. Conversely, the 2D-array substrate displayed a red-shifted and broadened absorption peak compared with that of the dot-type substrate. This behavior is known to occur when Au NPs are in contact with each other. Both substrates could excite SP with the 532 nm laser used in this study. Our previous work showed that substrates capable of inducing SP excitation exhibit significant enhancement effects in surface-enhanced Raman scattering measurements.[26] In addition, a positive correlation was found between the signal intensities of surface-enhanced Raman scattering and SALDI-MS when CV molecules were used as samples.[16] Therefore, we expected both substrates to

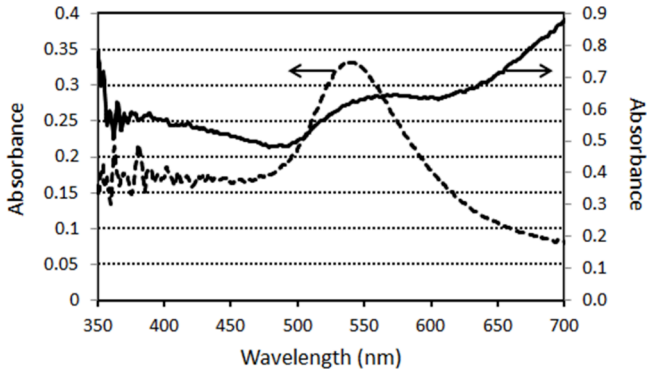

Figure 2. Absorption spectra of Au NPs/Si substrates: the dot-like substrate (dashed line, left axis) and 2D-array substrate (solid line, right axis).

demonstrate a signal enhancement effect in SALDI-MS measurements.

Figure 3a shows the SALDI-MS spectrum of CV molecules on a Si wafer prepared by using the drop method. As shown in Figure 3a, Na^+ (m/z = 23), K^+ (m/z = 39), and impurities were detected; however, no ions related to the CV molecules were detected. This result indicates that under these measurement conditions, the direct optical absorption by the CV molecule at 532 nm had no effect on the detection of CV molecules by SALDI-MS. Figure 3b,d shows the SALDI-MS spectrum of CV molecules on an Au NP dot-like substrate prepared using the drop method. Several peaks detected in this spectrum were attributed to nondissociated CV ions (m/z = 372) and dissociated CV ions (m/z = 358, 344, 330, 328, 316, 314, 302, 300, 288, and 286). An m/z difference of 14 corresponds to methyl groups ($-CH_2$) as the CV molecules have six methyl groups.[27] The ions at m/z = 328, 314, 300, and 286 are 2 smaller than the ions at m/z = 330, 316, 302, and 288, respectively, and may be dehydrated species. Figure 3c shows the SALDI-MS spectra of the CV molecules on the Au NP dot-like substrate prepared using the dip method. As shown in Figure 3c, more than half of the CV molecules were detected as nondissociated ions, and their intensity was more pronounced than that shown in Figure 3b. In these three SALDI-MS measurements, the fluence of the irradiating laser was the same (280 $\mu J/mm^2$); under the condition without Au NP dots, no CV-related ions were detected, as shown in Figure 3a; therefore, all detected ions in Figure 3b,c are considered to have received a signal enhancement effect by SP excitation.

Although the experimental conditions were the same except for the sample preparation method (drop or dip method), apparent differences were observed in the SALDI-MS spectral patterns and ion intensities, as shown in Figure 3b,c. In the drop method, after the CV solution was dropped and thoroughly dried, the surface of the dot-like substrate exhibited uneven coloration, and this substrate exhibited poor spot-to-spot reproducibility in SALDI-MS measurements. This uneven color indicates that when the substrate was prepared by the drop method, CV molecules were present on the Au NPs in various states, such as stacked and chemically or physically adsorbed. In this case, since charge interactions occur only with molecules directly adsorbed on the surface of the Au NPs, many of the stacked CV molecules cannot receive energy from the charge interactions.

However, when the substrate was prepared using the dip method, the spot-to-spot reproducibility was higher than that

https://doi.org/10.1021/acsomega.3c08648
ACS Omega 2024, 9, 21822−21828

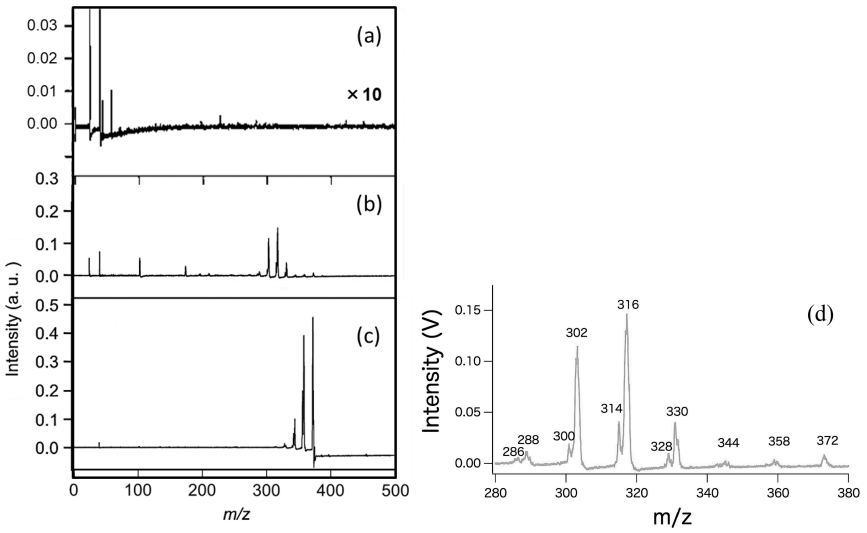

Figure 3. SALDI-MS spectra of CV molecules on a (a) Si wafer, (b) dot-like substrate prepared by the drop method, (c) dot-like substrate prepared by the dip method, and (d) a magnified view of (b). Laser fluence was set at 280 μJ. Each mass spectrum was integrated over 32 shots of measurements.

of the substrate prepared by the drop method, suggesting that the CV molecules were uniformly adsorbed on the Au NPs. This uniform adsorption of CV onto the Au NPs occurred because only chemisorbed CV molecules were present on the first layer of the Au NP surface, whereas the physically adsorbed CV molecules were washed away by the dip method. In this case, the CV molecules can receive energy through internal energy transfer and charge interactions. Therefore, the difference in the form of the energy supply based on the different adsorption conditions of the CV molecules on the Au NPs may be responsible for differences in the spectral patterns and signal intensities. We have previously reported that the desorption/ionization mechanism of Au NPs is related to local heating and charge interactions based on SP excitation.[16] Moreover, we reported that SP excitation with suppression of the internal energy supply reduces the fragmentation of sample molecules using SALDI-MS measurements with attenuated total reflection.[17] From these reports, we assumed that the differences in the fragment patterns between these two SALDI-MS spectra were due to the quantity of the supplied internal energy.

Here, we discuss the effect of the internal energy supply from the dot-shaped substrate to the CV molecules adsorbed on the surface on the spectral pattern when the sample is prepared using the dip method based on the measurement of the dependence of the SALDI-MS spectral pattern of the CV molecules on the laser fluence. Figure 4 shows the normalized SALDI-MS spectra of CV molecules under different laser fluences ranging from 80 to 280 μJ/mm^2. The small peak detected at a slightly higher m/z than that of nondissociated CV was attributed to the isotopic peak of CV and will not be discussed here. A higher laser fluence resulted in a larger total quantity of detected ions (amount and intensity) and a higher fragment ratio of dissociated to nondissociated CV ions (Table 1). The higher laser fluence provided a considerable amount of energy to the Au NPs through SP excitation; therefore, the increase in the fragment ratio can be attributed to the large amount of laser energy received. However, this result alone makes it difficult to discuss the relationship between the increase in the fragment ratio and energy supply.

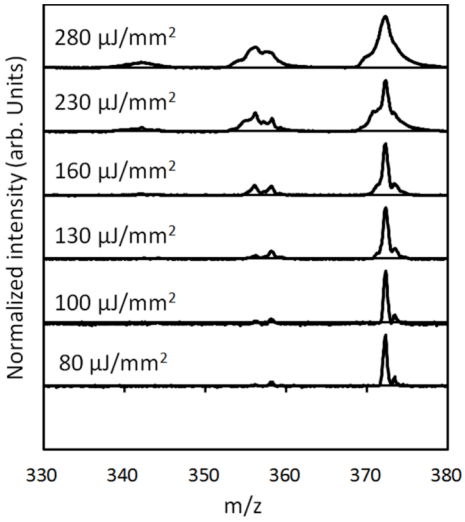

Figure 4. Normalized SALDI-MS spectra of CV molecules on the dot-like substrate prepared using the dip method under different laser fluences from 80 to 280 μJ/mm^2. Each mass spectrum was integrated over 32 shots of measurements.

We focused on the peak shape in more detail to further analyze the relationship between the laser fluence and the nondissociated CV ions at an m/z of 372. Figure 5 illustrates that at low laser fluence levels (80 and 100 μJ/mm^2), the peak was a single sharp component. However, the peak became a mix of sharp and broad components at intermediate and high fluences, respectively. Theoretically, ions with the same m/z should exhibit the same kinetic energy and flight time at the same accelerating voltage. However, the peak width broadened because of the distribution of the initial kinetic energy from the desorption of the sample before reaching the acceleration plates. In other words, the peak width reflects the kinetic energy distribution during desorption. Based on this consideration, the nondissociated CV ions at intermediate and higher fluences had two dispersed initial kinetic energies upon desorption from the dot-like substrate, suggesting that

https://doi.org/10.1021/acsomega.3c08648
ACS Omega 2024, 9, 21822−21828

Table 1. Effect of the Laser Fluence on the m/z = 372 Ion Intensity and Fragment Ratios of Dissociated to Nondissociated Ions by the Dip Method Using Dot-like or 2D-Array Substrates[a]

	peak ion intensity at m/z = -372 (V)		integrated intensity at m/z=372(-V)		fragment ratio of dissociated ions to nondissociated ions	
laser fluence (μJ/mm^2)	dot-like	2D-array	dot-like	2D-array	dot-like	2D-array
80	0.2	0.2	0.3	0.3	0.04	N.D.
100	0.6	0.4	0.9	0.7	0.05	N.D.
130	1.9	0.8	5.2	1.2	0.20	0.005
160	1.9	1.3	5.9	3.1	0.17	0.13
230	2.2	2.9	13.0	8.0	0.49	0.18
280	3.9	4.1	30.7	13.0	0.58	0.20

[a]Ion intensities are both the peak value signal intensity and the integrated intensity, which considers the peak width.

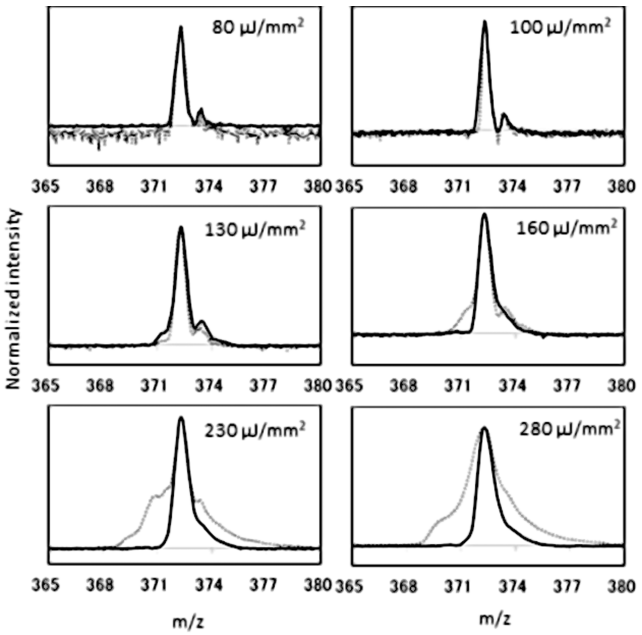

Figure 5. Comparison of normalized SALDI-MS spectra of CV molecules on the dot-like (dashed line) and the 2D-array (solid line) substrates prepared using the dip method under different laser fluences from 80 to 280 μJ/mm^2. Each mass spectrum was integrated over 32 shots of measurements.

the desorption/ionization process of the nondissociated CV ions on the dot-like substrate had two different mechanisms.

In contrast, the peaks at m/z values of 358 and 344 corresponding to the dissociated ions exhibited only broad components. Furthermore, all of the dissociated ions in Figure 3d also had only broad components. These dissociated ions are produced by an increase in the internal energy; therefore, the broad components of these SALDI-MS spectra may correspond to desorbed ions produced by the internal energy supply.

Table 1 shows the ion intensity and number of ions at an m/z of 372 and fragment ratio of dissociated ions to nondissociated ions for both the dot-like and 2D-array substrates. These two ionization substrates had comparable signal intensities for a nondissociated ion at m/z = 372 under all laser fluence conditions. Regarding the integrated intensity of the peaks, there is a significant increase in the integrated intensity for the dot-like substrate with increasing laser fluence, attributable to the broad components mentioned above. The 2D-array substrate has ten times more CV molecules than the dot-like substrate per SALDI-MS measurement because the number of monolayered CV molecules is proportional to the total surface area of Au NPs in the irradiated laser spot. Regarding the signal intensity, the dot-like substrate demonstrated a better desorption/ionization efficiency compared to the 2D-array ionization substrate. The 2D-array ionization substrate can overcome the disadvantages of its lower desorption and ionization efficiency by increasing the effective surface area of the ionization substrate.

However, the fragment ratio of the 2D-array substrate became much smaller than that of the dot-like substrate with increasing laser fluence. This result indicates that the Au NP array affects the soft desorption/ionization capacity of the sample in the SALDI-MS measurement, because the experimental conditions for sample preparation and laser irradiation are almost identical. The arrangement of Au NPs on the 2D-array substrate may suppress thermal energy transfer from the SP-excited Au NPs to the CV molecules because excessive internal energy transfer contributes significantly to the fragmentation of the sample molecules.

One Au NP in the 2D-array ionization substrate was in contact with air, SiO_2 (oxide layer of the Si wafer), CV molecules, and other Au NPs, as shown in Figure 1b. Among these materials, Au exhibits the highest thermal conductivity (314 W/mK).[28] Therefore, we assumed that almost all of the internal energy stored in one Au NP through SP excitation diffused to neighboring Au NPs. In contrast, in the dot-like substrate, most of the Au NPs did not come into contact with other Au NPs. Therefore, the thermal energy stored in one Au NP resulting from SP excitation should dissipate to the SiO_2 surface because SiO_2 has the highest thermal conductivity value of 1 W/mK among these materials.[29] Nevertheless, the thermal conductivity of SiO_2 is much lower than that of Au. Consequently, the amount of thermal energy that diffused from one Au NP to the SiO_2 surface was significantly lower than that that diffused to neighboring Au NPs, and the Au NP surface temperature in the dot-like ionization substrate was much higher immediately after laser irradiation than that in the 2D-array ionization substrate. Therefore, a higher temperature of the dot-like ionization substrate is believed to lead to a higher fragment ratio than that of the 2D-array ionization substrate.

Additionally, previous research has indicated that the lifetime of the SP phenomenon is very short, lasting less than one picosecond. Moreover, our previous study demonstrated that electrons excited by SP caused charge interactions between the sample molecules and surfaces of Au NPs within 200 fs.[21] Therefore, the electrons involved in SP excitation could not diffuse to distant locations and immediately interacted with the sample molecules on the Au NP surface. In contrast, thermal diffusion from the Au NPs to the surrounding medium occurs on a time scale ranging from subpicoseconds to nanoseconds. These considerations suggest that the 2D-array substrate suppresses the supply of thermal energy in the SALDI-MS measurements.

From these discussions, the Au NP surfaces used as SALDI-MS substrates supply two types of energy: thermal energy and charge interaction. Thermal energy is a good desorption/

https://doi.org/10.1021/acsomega.3c08648
ACS Omega 2024, 9, 21822−21828

ionization source; however, excess thermal energy leads to the dissociation of sample molecules and reduced m/z resolution. On the other hand, charge interaction caused no broadening of the nondissociated ion peak. The dot-like substrate produced a high S/N ratio with fewer ions. The dot-like substrate can supply these two types of energy in ample quantities because of its significant absorbance of 532 nm laser irradiation and becomes a highly sensitive SALDI-MS substrate. However, the balance of these two types of energy generated on a dot-like substrate is not favorable for SALDI-MS measurements with soft ionization. However, the 2D-array ionization substrate, which overcomes the balance of these two types of energy, can be a useful SALDI-MS ionization substrate for high sensitivity and nondissociative SALDI-MS measurements among conventional SALDI-MS ionization substrates. This substrate is expected to enable a more practical analysis of sample molecules with low m/z values.

We performed SALDI-MS measurements of practical sample molecules using this 2D-array ionization substrate and the dip technique. Figures 6a, b, and c show the SALDI-MS spectra obtained for angiotensin II, substance P, and reserpine molecules, respectively, using the 2D-array ionization substrate with the dip preparation technique. Angiotensin II with a molecular weight of 1046.2 g/mol and substance P with a molecular weight of 1347.6 g/mol are peptide molecules commonly employed as standard LDI-MS samples, including MALDI-MS and SALDI-MS. As illustrated in Figure 6a,b, our SALDI-MS system enabled the detection of intact peptide ions such as $[M+H]^+$, $[M+Na]^+$, and $[M+K]^+$. Reserpine, with a molecular weight of 608.7 g/mol, is a medical agent frequently used in various medications such as ataractic and blood-pressure-lowering drugs. Figure 6c shows the detection of nondissociated reserpine ions at m/z 609 with sufficient sensitivity. The enlarged spectrum of reserpine in Figure 6c shows several peaks around m/z 607, which correspond to ionized dehydrogenated forms of reserpine and not dissociated reserpine molecules.[30] Furthermore, reserpine is a molecule where fragment ions are easily observed at m/z 195 and 397,[31] but few of these fragment ions were observed. This indicates that our SALDI-MS measurement system provides a soft ionization/desorption process.

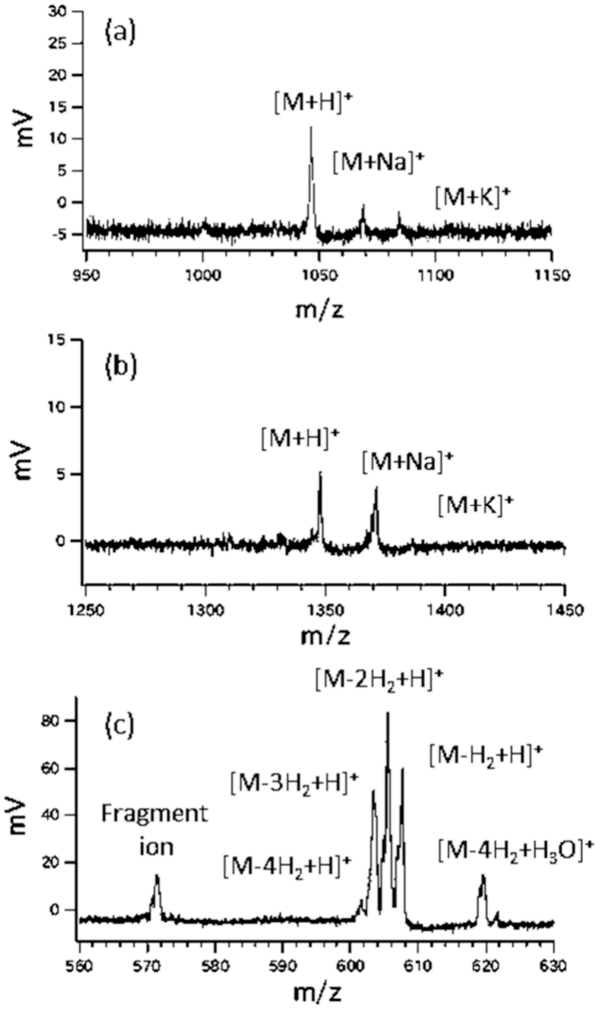

Figure 6. SALDI-MS spectra of (a) angiotensin II, (b) substance P, and (c) reserpine molecules on a 2D-array substrate prepared by the dip method. Each mass spectrum was integrated over 32 shots of measurements.

CONCLUSIONS

In summary, we compared two types of ionization substrates, a dot-like substrate and a 2D-array substrate, for SALDI-MS measurements. The dot-like substrate consisted of randomly dispersed Au NPs on a silicon wafer, while the 2D-array substrate contained Au NPs arranged in a two-dimensional array. The reflectance spectra of the substrates showed differences in optical absorption, owing to the arrangement of the Au NPs. Both substrates were expected to enhance the signal in SALDI-MS measurements. The experimental results revealed that using the dip method for sample preparation on the 2D-array substrate yielded better reproducibility and more uniform adsorption of the sample molecules compared to the drop method on the dot-like substrate. The desorption-ionization mechanism of the Au NPs is related to local heating and charge interaction based on SP excitation. A higher laser fluence increased the total quantity of ions detected and the fragment ratio of the dissociated ions. The dot-like substrate showed a higher desorption/ionization efficiency but also a higher fragment ratio than the 2D-array substrate. The arrangement of Au NPs in the 2D-array substrate suppressed internal energy transfer and reduced fragmentation. The 2D-array substrate demonstrates soft ionization and desorption capabilities and is suitable for SALDI-MS measurements of various sample molecules with high sensitivity and reproducibility.

AUTHOR INFORMATION

Corresponding Author

Kohei Shibamoto − *Department of Chemistry, Graduate School of Science, Tokyo Metropolitan University, Tokyo 192-0397, Japan;* orcid.org/0000-0003-2559-6739; Phone: +81-42-677-2531; Email: shiba@tmu.ac.jp

Author

Takashi Fujita − *Department of Applied Chemistry, School of Engineering, Tokyo University of Technology, Tokyo 192-0982, Japan*

Complete contact information is available at: https://pubs.acs.org/10.1021/acsomega.3c08648

https://doi.org/10.1021/acsomega.3c08648
ACS Omega 2024, 9, 21822−21828

Author Contributions

The manuscript was written with contributions from all authors. All the authors approved the final version of the manuscript.

Funding

JP18K04730 (Kohei Shibamoto) and JP19K15410 (Takashi Fujita).

Notes

The authors declare no competing financial interest.

■ ACKNOWLEDGMENTS

The authors thank M. Tani for her technical assistance with the experiments. This work was supported by JSPS KAKENHI, grant numbers JP18K04730 (Kohei Shibamoto) and JP19K15410 (Takashi Fujita)

■ REFERENCES

(1) Law, K. P.; Larkin, J. R. Recent advances in SALDI-MS techniques and their chemical and bioanalytical applications. *Anal. Bioanal. Chem.* **2011**, *399*, 2597−2622.
(2) Silina, Y. E.; Volmer, D. A. Nanostructured solid substrates for efficient laser desorption/ionization mass spectrometry (LDI-MS) of low molecular weight compounds. *Analyst.* **2013**, *138*, 7053−7065.
(3) Lakab, S. A.; Rafols, P.; García-Altares, M.; Yanes, O.; Correig, X. Silicon-based laser desorption ionization mass spectrometry for the analysis of biomolecules: A progress report. *Adv. Funct. Mater.* **2019**, *29*, No. 1903609.
(4) Hillenkamp, F.; Karas, M.; Beavis, R. C.; Chait, B. T. Matrix-assisted laser desorption/ionization mass spectrometry of biopolymers. *Anal. Chem.* **1991**, *63*, 1193A−1203A.
(5) Wei, J.; Buriak, J. M.; Siuzdak, G. Desorption−ionization mass spectrometry on porous silicon. *Nature* **1999**, *399*, 243−246.
(6) Shen, Z.; Thomas, J. J.; Averbuj, C.; Broo, K. M.; Engelhard, M.; Crowell, J. E.; Finn, M. G.; Siuzdak, G. Porous silicon as a versatile platform for laser desorption/ionization mass spectrometry. *Anal. Chem.* **2001**, *73*, 612−619.
(7) Okuno, S.; Wada, Y.; Arakawa, R. Quantitative analysis of polypropyleneglycol mixtures by desorption/ionization on porous silicon mass spectrometry. *Int. J. Mass Spectrom.* **2005**, *241*, 43−48.
(8) Lo, C. Y.; Lin, J. Y.; Chen, W. Y.; Chen, C. T.; Chen, Y. C. Surface-assisted laser desorption/ionization mass spectrometry on titania nanotube arrays. *J. Am. Soc. Mass Spectrom.* **2008**, *19*, 1014−1020.
(9) Combaret, V.; Bergeron, C.; Bréjon, S.; Iacono, I.; Perol, D.; Négrier, S.; Puisieux, A. Protein chip array profiling analysis of sera from neuroblastoma patients. *Cancer Lett.* **2005**, *228*, 91−96.
(10) Seino, T.; Sato, H.; Yamamoto, A.; Nemoto, A.; Torimura, M.; Tao, H. Matrix-free laser desorption/ionization-mass spectrometry using self-assembled germanium nanodots. *Anal. Chem.* **2007**, *79*, 4827−4832.
(11) Kawasaki, H.; Yonezawa, T.; Watanabe, T.; Arakawa, R. Platinum nanoflowers for surface-assisted laser desorption/ionization mass spectrometry of biomolecules. *J. Phys. Chem. C* **2007**, *111*, 16278−16283.
(12) Pilolli, R.; Palmisano, F.; Cioffi, N. Gold nanomaterials as a new tool for bioanalytical applications of laser desorption ionization mass spectrometry. *Anal. Bioanal. Chem.* **2012**, *402*, 601−623.
(13) Palermo, A.; Forsberg, E. M.; Warth, B.; Aisporna, A. E.; Billings, E.; Kuang, E.; Benton, H. P.; Berry, D.; Siuzdak, G. Fluorinated gold nanoparticles for nanostructure imaging mass spectrometry. *ACS Nano* **2018**, *12*, 6938−6948.
(14) Ràfols, P.; Vilalta, D.; Torres, S.; Calavia, R.; Heijs, B.; McDonnell, L. A.; Brezmes, J.; del Castillo, E.; Yanes, O.; Ramírez, N. I.; Correig, X. Assessing the Potential of Sputtered Gold Nanolayers in Mass Spectrometry Imaging for Metabolomics Applications. *PLoS One* **2018**, *13*, No. e0208908.
(15) Huang, Y. F.; Chang, H. T. Analysis of Adenosine Triphosphate and Glutathione through Gold Nanoparticles Assisted Laser Desorption/Ionization Mass Spectrometry. *Anal. Chem.* **2007**, *79*, 4852−4859.
(16) Shibamoto, K.; Sakata, K.; Nagoshi, K.; Korenaga, T. Laser desorption ionization mass spectrometry by using surface plasmon excitation on gold nanoparticle. *J. Phys. Chem. C* **2009**, *113*, 17774−17779.
(17) Shibamoto, K.; Nishimura, Y.; Fujita, T. Study of surface plasmon-assisted LDI-MS measurement with attenuated total reflection. *Chem. Lett.* **2016**, *45*, 262−264.
(18) Huang, W.; Lai, S. K.-M.; Liang, K.; Pu, K.; Wang, X.; Chen, Y.; Ng, K.-M. Near-Field-Induced Ionization on Photo-Excited Gold Nanoparticles. *J. Phys. Chem. C* **2023**, *127*, 10508−10514.
(19) Fujita, T.; Shibamoto, K. Titania surface-assisted laser desorption−ionization mass spectrometry of oligosaccharides. *Chem. Lett.* **2013**, *42*, 852−853.
(20) Shibamoto, K.; Katayama, K.; Fujinami, M.; Sawada, T. Fundamental processes of surface enhanced Raman scattering detected with transient reflecting grating spectroscopy. *Rev. Sci. Instrum.* **2003**, *74*, 910−912.
(21) Shibamoto, K.; Katayama, K.; Sawada, T. Ultrafast charge transfer in surface-enhanced Raman scattering (SERS) processes using transient reflecting grating (TRG) spectroscopy. *Chem. Phys. Lett.* **2007**, *433*, 385−389.
(22) Nagoshi, K.; Shibamoto, K. Optimization of added solvent in the two-dimensional arraying of gold nanoparticles in aqueous solution evaluated by laser desorption/ionization mass spectra. *Bunseki Kagaku* **2014**, *63*, 9−15.
(23) Shibamoto, K.; Yasumuro, K.; Horiuchi, T.; Teraoka, T.; Fujita, T. Study of Two-dimensional Highly-ordering of Gold Nanoparticles for an Optical Sensor Using Surface Plasmon Excitation as an Assistance Effect. *Bunseki Kagaku* **2014**, *63*, 293−298.
(24) Zhang, K.; Zeng, T.; Tan, X.; Wu, W.; Tang, Y.; Zhang, H. A facile surface-enhanced Raman scattering (SERS) detection of rhodamine 6G and crystal violet using au nanoparticle substrates. *Appl. Surf. Sci.* **2015**, *347*, 569−573.
(25) Wan, L.; Shundo, S.; Inukai, J.; Itaya, K. Ordered Adlayers of Organic Molecules on Sulfur-Modified Au(111): In Situ Scanning Tunneling Microscopy Study. *Langmuir.* **2000**, *16*, 2164−2168.
(26) Fujita, T.; Shibamoto, K. Formation and characterization of 2D closely packed arrays of bare gold nanoparticles without aggregation. *ACS Omega* **2022**, *7*, 44711−44719.
(27) Weyermann, C.; Kirsch, D.; Costa Vera, C.; Spengler, B. Evaluation of the Photodegradation of Crystal Violet upon Light Exposure by Mass Spectrometric and Spectroscopic Methods. *J. Forensic Sci.* **2009**, *54*, 339−345.
(28) Langer, G.; Hartmann, J.; Reichling, M. Thermal conductivity of thin metallic films measured by photothermal profile analysis. *Rev. Sci. Instrum.* **1997**, *68*, 1510−1513.
(29) Callard, S.; Tallarida, G.; Borghesi, A.; Zanotti, L. Thermal conductivity of SiO_2 films by scanning thermal microscopy. *J. Non-Cryst. Solids* **1999**, *245*, 203−209.
(30) Yamagaki, T.; Osawa, T.; Fujikawa, K.; Watanabe, T.; Sugahara, K. Multimatrix Variation Matrix-Assisted Laser Desorption/Ionization Mass Spectrometry as a Tool for Determining the Bonding of Nitrogen Atoms in Alkaloids. *J. Am. Soc. Mass Spectrom.* **2022**, *33* (12), 2243−2249.
(31) Alimpiev, S.; Grechnikov, A.; Sunner, Y.; Karavanskii, V.; Simanovsky, Y.; Nikiforv, S. Surface-assisted laser desorption/ionization mass spectrometry with a rotating ball interface. *Rapid Commun. Mass Spectrom.* **2011**, *25*, 140−146.

https://doi.org/10.1021/acsomega.3c08648
ACS Omega 2024, 9, 21822−21828